

A Rotation Meanout Network with Invariance for Dermoscopy Image Classification and Retrieval

Yilan Zhang^a, Fengying Xie^{a,*}, Xuedong Song^b, Hangning Zhou^a, Yiguang Yang^a, Haopeng Zhang^a, Jie Liu^c

^aImage Processing Center, School of Astronautics, Beihang University, Beijing 100191, China

^bShanghai Aerospace Control Technology Institute, Shanghai 201109, China

^cDepartment of Dermatology, Peking Union Medical College Hospital, Chinese Academy of Medical Sciences and Peking Union Medical College, Beijing 100730, China

Abstract

The computer-aided diagnosis (CAD) system can provide a reference basis for the clinical diagnosis of skin diseases. Convolutional neural networks (CNNs) can not only extract visual elements such as colors and shapes but also semantic features. As such they have made great improvements in many tasks of dermoscopy images. The imaging of dermoscopy has no main direction, indicating that there are a large number of skin lesion target rotations in the datasets. However, CNNs lack anti-rotation ability, which is bound to affect the feature extraction ability of CNNs. We propose a rotation meanout (RM) network to extract rotation invariance features from dermoscopy images. In RM, each set of rotated feature maps corresponds to a set of weight-sharing convolution outputs and they are fused using meanout operation to obtain the final feature maps. Through theoretical derivation, the proposed RM network is rotation-equivariant and can extract rotation-invariant features when being followed by the global average pooling (GAP) operation. The extracted rotation-invariant features can better represent the original data in classification and retrieval tasks for dermoscopy images. The proposed RM is a general operation, which does not change the network structure or increase any parameter, and can be flexibly embedded in any part of CNNs. Extensive experiments are conducted on a dermoscopy image dataset. The results show our method outperforms other anti-rotation methods and achieves great improvements in dermoscopy image classification and retrieval tasks, indicating the potential of rotation invariance in the field of dermoscopy images.

Keywords: Dermoscopy, Image classification, Image retrieval, Rotation invariance, Convolutional neural networks

1. Introduction

Skin is the organ with the largest area and the closest contact with the outside world in the human body. As a strong physiological barrier, the skin plays a key role in protecting human health [1]. Today, skin disease has become a common disease worldwide and a major public health problem [2]. Dermoscopy is a non-invasive microscopic image analysis technique that can magnify the area of skin lesions dozens of times, helping doctors to observe the fine structures and pigments under the skin surface [3]. The use of dermoscopy assistance can effectively improve the diagnostic accuracy [4]. However, the diagnostic results are highly dependent on the experience of dermatologists and are less reproducible [5]. Therefore, with the increasing number of skin disease cases worldwide, the demand for remote automatic diagnosis solutions has become more and more important [6].

With the maturity of computer technology, the biomedical scientific community is increasingly interested in computer-supported skin lesion examination and characterization [7]. The computer aided diagnosis (CAD) system can extract the features representing the original dermoscopy data, and use these quantified features for tasks such as skin lesions classification and retrieval, to provide a more reliable diagnosis basis for clinical works and have a

*Corresponding author

Email address: xfy_73@buaa.edu.cn (Fengying Xie)

far-reaching impact on dermatology clinic [8]. Features with better separability can effectively represent dermoscopy data and eliminate irrelevant information, which largely determines the success of subsequent tasks.

The early used features are hand-crafted features [9; 10], which are usually low-level features, do not have semantic information, and are less robust. During the past decade, the field of deep learning has developed vigorously. Among the studies, convolutional neural network (CNN) provides a learning-based solution for image feature extraction, which can effectively avoid the shortcomings of manual features, and has been widely used in dermoscopy image analysis [11], for example the works in [12; 13; 14; 15; 16].

Although CNNs have shown their effectiveness in the tasks of dermoscopy image classification [14; 15], retrieval [17; 16], segmentation [18] and so on with its ability of automatic feature learning. The rotation often happens in the process of capturing dermoscopy images which are non-directional. Besides the pooling layer endows CNNs the scalability for small image rotation, CNNs have weak anti-rotation capability[19]. So the rotation transformation would bring about an adverse impact on the feature learning process. The type of skin disease does not change due to the dermoscopy imaging angle. This requires the extracted features to have certain invariance to rotation transformation.

Therefore, this paper adopts the deep learning method to study the rotation-invariant feature extraction of dermoscopy images. We proposed a novel general operation, namely rotation meanout (RM), which expands the input feature maps by rotating them at equal interval angles, and then fuses these expanded feature maps using meanout operation. We used representative images dataset provided by International Skin Imaging Collaboration (ISIC) 2019 classification challenge [20; 21; 22], which is also called ISIC 2019 dataset. On this dataset, we analyzed the factors influencing the RM's performance and verified that through RM, dermoscopy features can be effectively extracted, which can help get better performance in classification and retrieval tasks.

The contributions of this paper are three-fold: (1) We propose a new network for dermoscopy image feature extraction, RM, to solve the problem of a large number of skin lesion target rotations in the dermoscopy dataset. It is theoretically proven that RM is rotation-equivariant, even rotation-invariant when being followed by the global average pooling (GAP) operation. (2) The proposed RM network does not change the network structure or increase the network parameters. It can be flexibly combined with any part of a CNN and effectively improves the rotation invariance ability of the CNNs. (3) We verified the effectiveness of the RM in dermoscopy image classification and retrieval tasks, respectively, demonstrating its validity and generality. Through experimental verification, the effect of RM is better than the other classic rotation invariance or equivariance methods commonly used in natural images. Compared with other skin lesion classification and retrieval methods, RM also achieves great performance.

2. Related Works

2.1. Dermoscopy Image Feature Extraction Based on CNNs

In recent years, CNNs with hierarchical feature learning capability have made breakthroughs in dermoscopy image feature extraction. Kawahara *et al.*[12] presented a fully convolutional neural network based on AlexNet [23] to extract representative features of melanoma. Yu *et al.*[13] used ResNet34 [24] as the network architecture in the classification stage. With the continuous proposal of new network structures, SENet [25], EfficientNet [26], RegNet[27], etc. can also be used as feature extraction network [14]. Although these methods have achieved better performance than those based on hand-crafted features, they are mainly designed for natural images such as ImageNet. Some studies have improved the network structure for dermoscopy image characteristics, thereby enhancing the discriminative representation ability of CNNs. Zhang *et al.*[15] proposed an attention residual learning (ARL) mechanism to make the network focus on the area of skin lesions. Another attention model called a hybrid dilated convolution spatial attention (HDCSA) is inserted into the network, which can not only extract global features but also detailed features of skin lesions [16]. However, none of the above methods take into account the characteristic that the skin lesions have no main direction.

2.2. Rotation Invariance Features Extraction of CNNs

Good features should be with invariance in image classification and retrieval tasks [28]. This is because that in image classification task, the category label of the image does not change as the position of the classified object changes in the image, and in image retrieval task, the distance between features of the intra-class is expected to be smaller,

even if there are some image transformations. Local connection, weight sharing and pooling operation in CNNs can provide translation invariance[29] and the multilayer structure of CNNs expands the receptive field to provide scale invariance. However, CNNs have weak rotation invariance capability, resulting in the weak generalization ability of the model. Some scholars have proposed methods to solve this problem. These methods are mainly based on data augmentation, rotating convolution kernels and anti-transformation.

Rotating images is a simple way to improve the rotation-invariant capability of CNNs, among which rotation augmentation [30] is commonly used. TI-Pooling [31] input the considered transformation set to a parallel siamese architecture and fused the outputs of several branches using a pooling strategy. Another idea is to exploit the translation invariance of CNNs by using polar mapping to convert rotation to translation of the input image [32]. This kind of method pay more attention to learning the features from the enriched inputs with the risk of overfitting [33]. The second kind of method usually rotates the filters to obtain the feature maps of different orientation channels and fuses them to obtain the rotation-equivariant or rotation-invariant features. For example, Marcos *et al.*[34] encoded rotation invariance by simply rotating the convolutional kernels. Cohen *et al.*[35] introduced group equivariant convolutional neural networks (GCNNs), which obtained the anti-rotation ability by repeating the transformed filters at different rotation-flip combinations. Zhou *et al.*[36] proposed an oriented response network (ORN) which used Active Rotating Filters (ARFs) to explicitly encode the location and orientation information of feature maps. After that, some new methods were raised on this basis [37; 38]. The methods based on rotating convolution kernels usually use new convolution layers to replace the traditional ones. However, the sizes of filters are usually small and features are easily influenced by the interpolation errors. Anti-transformation methods[39; 40] take rotation as a special case of transformation. For example, Jaderberg *et al.*[39] proposed a spatial transformation network (STN) to incorporate global transformation invariance into the network, but STN does not have a strictly invariant.

Recently, a large number of researches based on the rotation equivariance and variance focus on the fields including remote sensing images [41], 3D point clouds[42], face detection [43], molecular representation [44], etc. However, there are few studies on dermoscopy images, and the effectiveness of the rotation invariance methods in skin lesion classification and retrieval remains to be verified.

2.3. Rotation Invariance Features for Dermoscopy Images

In recent years, a few of scholars have gradually noticed the importance of rotation-invariant features in the field of dermoscopy images tasks. Li *et al.*[45] introduced GCNNs [35], and proposed G-upsampling and G-downsampling for the task of skin lesion segmentation. This method makes the network have certain rotation equivariance but may also introduce interpolation errors. Based on the rotation-invariant deep hashing network [16], the Cauchy rotation loss function is designed, which is mainly aimed at the retrieval task of dermoscopy images and the method of rotating the input requires more calculation. Despite the success of rotation invariance studies in natural images tasks, research on rotation-invariant features in dermoscopy images still has great potential.

3. Methodology

CNNs lack the rotation invariance [31]. Although many scholars have made some progress in this field, their methods have problems such as increasing the number of model parameters and changing the network structure, and the applicability of the dermoscopy image task remains to be verified. To overcome these limitations, we proposed a new network called rotation meanout (RM), to improve the feature extraction ability on rotations of the networks. Our proposed RM does not change the network structure or increase parameters, which is easily implemented. Besides, RM is a general model and can be flexibly combined with any part of a CNN.

3.1. The Proposed RM Network

Let $X = [x_0, x_1, \dots, x_n]$ be a set of input feature maps with numbers of n , the proposed RM model can be described as follows:

$$RM(X) = p[f(X), r_{\theta}^{-1}f(r_{\theta}X), r_{2\theta}^{-1}f(r_{2\theta}X), \dots, r_{(k-1)\theta}^{-1}f(r_{(k-1)\theta}X)] \quad (1)$$

Where $f(\cdot)$ represents a convolution operation to extract features, $r_{i\theta}$ ($i \in [0, k)$) represents rotating $i \cdot \theta$ degrees clockwise and $r_{i\theta}^{-1}$ represents rotating $i \cdot \theta$ degrees counterclockwise, k denotes the number of rotation and is subject to $k \cdot \theta = 360^\circ$, p stands for a fusion operation.

Figure 1 shows the flow chart of the RM network, which has four steps: expanding, feature extraction, realign, and fusion. Firstly, feature maps are expanded k times by rotating them at equal interval angles. Different from data

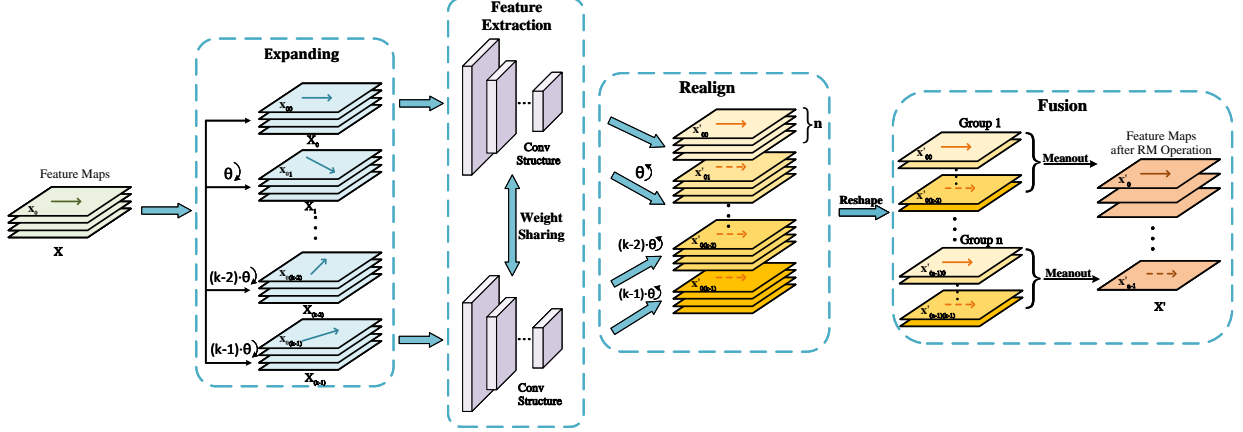


Figure 1: RM network. In expanding stage, feature maps are expanded k times by rotating them at same interval angles θ . In realign stage, the k groups of rotated feature maps are input to a shared convolutional structure to extract features. Then, inversely rotate the feature map back to its original angle, so that the outputs can be realigned to keep their spatial position relation. Finally, these k sets of realigned feature maps are fused to obtain one set of final feature maps by using the mean pooling operation.

rotation augmentation which rotates the original images, here we rotate the feature maps by $i \cdot \theta$ ($i = 0, 1, \dots, k - 1$) degrees before feeding them into the convolution layer. Interpolation is needed to complete the rotation operation for the feature maps. When the interpolation coordinate is not an integer, interpolation error will be introduced. Usually, as the depth of the CNNs increase, the size of the feature maps will continuously decrease, and the error will be more obvious.

Secondly, one set of feature maps each time, the k sets of rotated feature maps are sequentially input to a shared convolutional structure to extract features. The convolutional structure can be a simple or several convolutional layers, and even any more complex structure like an Inception Block in GoogLeNet [46] and a residual block in ResNet[24], etc. Weight sharing strategy is used during the process of training the shared convolutional structure, which does not change the original convolutional structure or increase any parameter.

Thirdly, the k sets of new feature maps output by the shared convolutional structure are realigned to keep their spatial position relation. Formula 1 can be written as the multiplied form of two vectors:

$$RM(X) = p[[1, r_{\theta}^{-1}, r_{2\theta}^{-1}, \dots, r_{(k-1)\theta}^{-1}] \circ [f(X), f(r_{\theta}X), f(r_{2\theta}X), \dots, f(r_{(k-1)\theta}X)]] \quad (2)$$

In (2), vector $[1, r_{\theta}^{-1}, r_{2\theta}^{-1}, \dots, r_{(k-1)\theta}^{-1}]$ is exactly the realign operation. That is, after the convolutions, the i^{th} ($i \in [0, k)$) set of rotated feature maps are realigned through rotating correspondingly counterclockwise by $i \cdot \theta$.

Finally, we fuse these k sets of realigned feature maps to obtain one set of final feature maps by using the orientation mean pooling operation:

$$p_{mean}(X) = mean[X'_0, X'_1, \dots, X'_{k-1}] \quad (3)$$

where X'_i ($i \in [0, k)$) represents the i^{th} set of feature maps after realign step. This set of final feature maps has the same number of channels as the original output of the shared convolutional structure, which can keep the network structure not change when the RM is embedded in a baseline network.

3.2. Analysis of RM

3.2.1. Rotation Equivariance and Rotation Invariance

It can be proved that the proposed network is rotation-equivariant to the input feature maps X . Rotation equivariance means that when the input is rotated, the learnt feature maps also change in a predictable way [47]. More formally, a function f is equivariant to a class of transformations T . If for all transformation $t \in T$ of the input X , a corresponding transformation t' of the output $f(X)$ can be found, so that $f(tX) = t'f(X)$ for all X citeschmidt2012learning.

From (2) we have:

$$\begin{aligned}
RM(r_\theta X) &= p[f(r_\theta X), r_\theta^{-1}f(r_{2\theta}X), r_{2\theta}^{-1}f(r_{3\theta}X), \dots, r_{(k-1)\theta}^{-1}f(r_{k\theta}X)] \\
&= r_\theta \cdot p[r_\theta^{-1}f(r_\theta X), r_{2\theta}^{-1}f(r_{2\theta}X), r_{3\theta}^{-1}f(r_{3\theta}X), \dots, r_{k\theta}^{-1}f(r_{k\theta}X)]
\end{aligned} \tag{4}$$

Because $k \cdot \theta = 360^\circ$, therefore $r_{k\theta}^{-1}f(r_{k\theta}X) = f(X)$, and (4) can be rewrite as:

$$RM(r_\theta X) = r_\theta \cdot RM(X)$$

Thus we have:

$$RM(r_{i\theta}X) = r_{i\theta} \cdot RM(X), i \in [0, k] \tag{5}$$

From (5), the proposed RM is rotation-equivariant.

Since many CNNs have a global average pooling (GAP) operation before the fully connected layers, which enforces each feature map to be a feature point and discards all of the spatial information. Let $GAP(\cdot)$ denotes the GAP operation, we have:

$$GAP(RM(r_{i\theta}X)) = GAP(r_{i\theta} \cdot RM(X)) = GAP(RM(X)) \tag{6}$$

Therefore, the GAP operation in classification and retrieval tasks makes the proposed RM network having rotation invariance, which reduces the influence of the angle changes of input images on the results.

3.2.2. Weight Sharing Strategy

In CNNs, the weight sharing of a convolution kernel is used to calculate convolution on an original image or on a set of feature maps, which reduces the parameters, and more important, the mined features have the ability of anti-translation. In the proposed RM network, all sets of the rotated feature maps are sequentially input to the convolutional structure and the weights are shared. The weight sharing strategy does not change the original convolutional structure or increase any parameter. And more important, because of the weight sharing strategy, RM has the property of rotation equivariance and rotation invariance.

3.3. Combine an RM with a CNN

The proposed RM does not change the dimensions of the input feature maps and can be easily embedded in a CNN. Figure 2 is two examples of embedding an RM operation in ResNet18 [24] (ResNet18 contains 8 residual blocks). In Figure 2 (a), four residual blocks from Res 5 to Res 8 are taken as the shared convolutional structure to be combined with the RM network. This is a strict RM-GAP structure (the RM is directly followed by the GAP operation), and the extracted features are rotation-invariant to the input feature maps of Res 5. In Figure 2 (b), only Res 5 is combined with the RM. This is a relaxed RM-GAP structure (the RM is separated with the GAP operation). Because the three residual blocks between Res 5 and GAP are not rotation-equivariant, the output by the GAP are also not rotation-invariant to the inputs of Res 5. Although the relaxed RM-GAP structure is not rotation-invariant, it still with good anti-rotation ability and can improve the network performance, which will be verified in our experiments. In fact, the proposed RM is a general model, and any convolutional block in CNNs can be taken as the basic unit and combined with an RM model.

4. Experiment

4.1. Implementation Details

In this paper, a general network RM was proposed, which can be easily embedded in a CNN and improve the network performance. We took four baseline networks including ResNet18, ResNet34, GoogleNet-Inception-V3[46] and EfficientNet-b0[26] to verify the effectiveness of the proposed RM network on the dermoscopy image dataset provided by International Skin Imaging Colaboration (ISIC) 2019 classification challenge, namely ISIC 2019 dataset. We conducted experiments on both classification task and retrieval task.

The networks were trained on a PC with two Nvidia GeForce GTX 1080Ti GPUs. The whole work was implemented with the PyTorch package. We use mini-batch stochastic gradient descent (SGD) optimization to train the

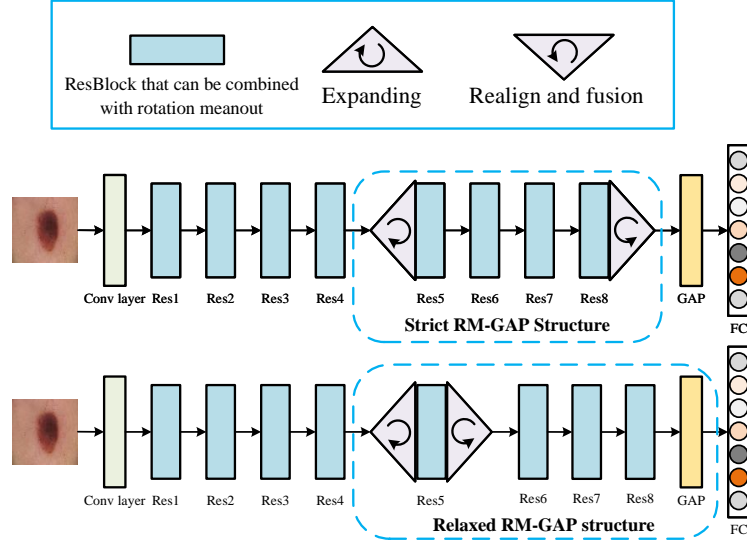


Figure 2: Embedding an RM in ResNet18.

models. The batch size was set to 32, and the weight decay and momentum were set to 0.0005 and 0.9, respectively. The transfer learning is used to initialize the CNNs with the model parameters pre-trained on the ImageNet. In classification task, the models were trained for 50 epoches, The initial learning rate was set to 0.01 and was reduced by 10 times after 20 and 40 epoches. While in retrieval task, the models were trained for 80 epoches. The learning rate was also set to 0.01 and was reduced by 10 times after 20, 40 and 60 epoches.

4.2. Evaluation Metrics

4.2.1. Classification Task

We use precision, sensitivity, specificity, and Kappa coefficient to evaluate the performance of classification task, as shown in the following formula respectively:

$$Precision = \frac{TP}{TP + FP} \quad (7)$$

$$Sensitivity = TPR = \frac{TP}{TP + FN} \quad (8)$$

$$Specificity = 1 - FPR = 1 - \frac{FP}{FP + TN} = \frac{TN}{FP + TN} \quad (9)$$

where TPR means true positive rate, FPR means false positive rate. TP , FN , TN and FP represent the number of true positive, false negative, true negative and false positive, respectively, and M denotes the number of classes. The higher the precision, sensitivity and specificity, the better the classification performance of the algorithms. The averaged value of each metric is reported for the evaluation, denoted as AP, Ave Sen and Ave Spec.

Moreover, we also use the Kappa coefficient [48] to measure the consistency of classification accuracy between results of different algorithms and it is derived as:

$$Kappa = \frac{p_0 - p_e}{1 - p_e} \quad (10)$$

where p_0 is the overall classification accuracy, p_e is the hypothetical probability of a chance agreement. Assuming that the numbers of real samples in each category are a_1, a_2, \dots, a_C and the predicted numbers of samples in each category are b_1, b_2, \dots, b_C , respectively, and the total number of samples is n , then p_0 and p_e can be expressed as:

$$p_0 = \frac{TN + TP}{TN + FP + FN + TP} \quad (11)$$

Table 1: Details of the ISIC 2019 dataset.

Category	Description	Sample Number	Proportion
MEL	Melanoma	4522	17.85%
NV	Melanocytic nevus	12875	50.83%
BCC	Basal cell carcinoma	3323	13.12%
AK	Actinic keratosis	867	3.42%
BKL	Benign keratosis	2624	10.36%
DF	Dermatofibroma	239	0.94%
VASC	Vascular lesion	253	1.00%
SCC	Squamous cell carcinoma	628	2.48%

$$p_e = \frac{a_1 \times b_1 + a_2 \times b_2 + \dots + a_C \times b_C}{n \times n} \quad (12)$$

When Kappa is greater than 0.75, the model has good consistency, when Kappa is between 0.40 and 0.75, it represents moderate consistency, and when Kappa is less than 0.40, it indicates that the model has poor consistency.

4.2.2. Retrieval Task

We use the mean average precision (mAP) and mean reciprocal rank (mRR) to evaluate the performance of the retrieval task, as shown in (13) and (14). The top 10 dermoscopy images in the retrieval stage are used as the final retrieval results.

$$\begin{aligned} mAP@10 &= \frac{1}{M} \sum_{c=1}^M \frac{1}{|Q_c|} \sum_{i=1}^{Q_c} \frac{TP_i}{TP_i + FP_i} \\ &= \frac{1}{M} \sum_{c=1}^M \frac{1}{|Q_c|} \sum_{i=1}^{Q_c} \frac{TP}{10} \end{aligned} \quad (13)$$

$$mRR@10 = \frac{1}{M} \sum_{c=1}^M \frac{1}{|Q_c|} \sum_{i=1}^{Q_c} \frac{1}{rank_i} \quad (14)$$

where Q_c is a set of query images with category c in the test set and $|Q_c|$ is the number of elements in the set. $rank_i$ is the ranking of the first correct matching image when retrieving the i -th image.

4.3. Dataset

ISIC 2019 dataset. The open dermoscopy dataset consists of 25,331 images across 8 different diagnostic categories with details in Table 1 and the sample images of each category are shown in Figure 3. We divide the dataset into the training set, validation set, and testing set according to the ratio 8:1:1. In addition, it is a dataset with unbalanced categories, therefore, we use the weighted cross-entropy as the loss function of the network. In this study, each original image in the training set is scaled to 256×256 by short edge, and a 224×224 crop is randomly sampled from it or its horizontal flip or vertical flip, with the per-pixel RGB scale to (0, 1) and mean value subtracted and standard variance divided. It needs to be indicated that rotation augmentation is not used here, to avoid the correlation between rotation augmentation and our RM network.

4.4. Verification of the Proposed Structure

We use ResNet18 as the baseline and the framework in Figure 2 (a) to verify the effectiveness of the proposed RM structure in skin lesion classification task.

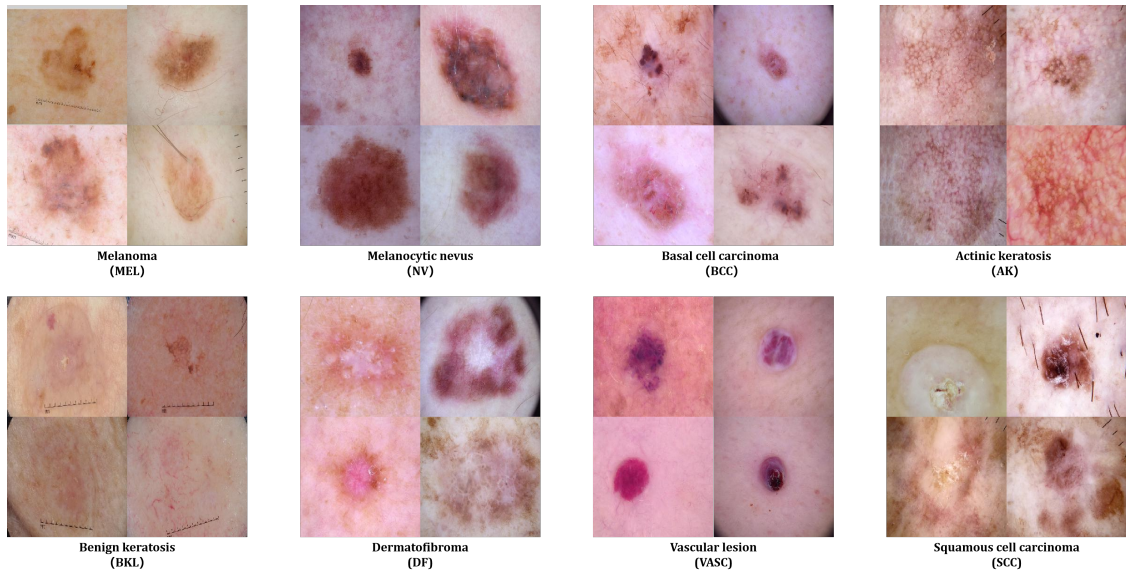


Figure 3: Sample images from the eight diagnostic categories.

Table 2: Ablation study on RM

Network	AP (%)	Ave Sen (%)	Ave Spec (%)
baseline	56.20	70.86	96.93
RM-WR	56.02	70.83	96.77
RM-NWS	57.36	72.96	97.08
RM	64.07	75.37	97.17

4.4.1. Ablation Study

We probe the effect of the proposed RM by ablation experiments. Table 2 presents the results of the ablation study, where RM represents the strict RM-GAP structure in Figure 2 (a), RM-WR means no rotation operations in the expanding and realign stages, RM-NWS denotes without weight sharing in the RM (each of rotation branches has an independent convolutional structure). It can be seen that module without rotation operation and the baseline have a similar performance within training error. For RM-NWS, the extracted features do not have rotation invariance, and the classification effect is less improved. Compared with the baseline, the module containing the rotation operation and using the weight sharing strategy has a significantly improved classification effect, in which the AP is increased by 7.87%, and the Ave Sen is increased by 4.51%. In addition, weight sharing has less local parameters, and thus significantly reduces model size.

We use the output of the classification layer as the features of the networks, and use the t-SNE[49] method to visualize it on the testing set. As we can see from the Figure 4, with RM, the distribution of the features is more dispersed in different categories and more aggregated within the same category, and the pink part is particularly obvious. In order to keep loss low during training, the sample distribution of minority classes will be scattered and the classifier performs worse. However, it can be seen from the red box that the RM can making the features of minority classes more compact (color cyan). Table 7 shows the metrics of each category, the precision of SCC increased from 22.58% to 32.26%, and the sensitivity increased from 60.87% to 64.52%. In summary, RM can improve the separability of features to a certain extent, whether the major classes or the minority classes.

4.4.2. Verification of Feature Fusion Strategy

Table 3 gives the results using three fusion strategies including maxout, meanout and embedding, where maxout outputs the maximum values of the corresponding positions in the feature maps, and embedding is to use 1×1

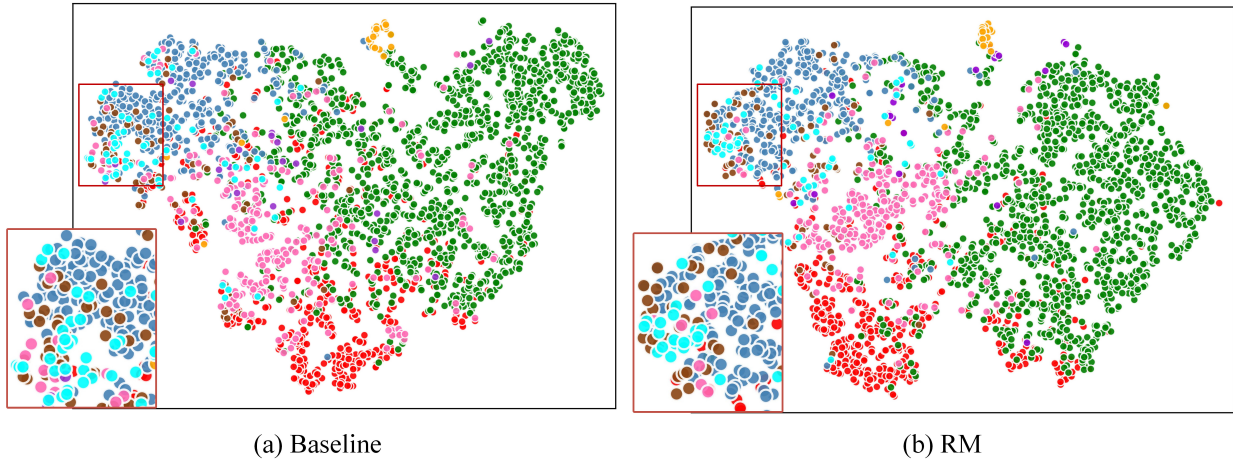


Figure 4: t-SNE visualization of the last layer representations of the networks, where (a) is the visualization of ResNet18 and (b) is that of ResNet18 combined with RM. (Refer to the legend in Figure 5 for the corresponding colors of skin diseases)

Table 3: The classification results of different fusion strategy

Network	AP (%)	Ave Sen (%)	Ave Spec (%)
Baseline	56.20	70.86	96.93
Embedding	60.04	73.10	96.77
Maxout	63.16	72.04	96.89
Meanout	64.07	75.37	97.17

convolution. It can be seen that all the three fusion strategies improved the classification performance to some degree. Different from maxout and meanout, when using embedding, the RM is not rotation-invariant and the AP is the lowest. Although the features extracted by maxout are also rotation-invariant, it may lead to the loss of feature continuity. Compared with maxout, meanout can preserve the features of the samples in different rotation angles better. Therefore, we selected meanout as the final fusion strategy in our RM network.

4.4.3. Verification of Rotation Intervals

Table 4 gives the classification results using different rotation intervals θ , including 90, 60 and 45 degrees. Bilinear interpolation was used during rotating the feature maps. For the rotation interval $\theta \neq 90^\circ$, we padded the boundary region of the feature maps using zero when performing clockwise rotation and then removed the uselessly surrounding region when performing rotating back (realignment), to avoid the information loss caused by rotation.

It can be seen from Table 4 that compared with ResNet18 baseline, RM with different rotation intervals all improve the performance of the network. Moreover, with the decrease of rotation angle interval, the index of AP increased gradually, but the sensitivity decreased gradually. Theoretically, the smaller the rotation interval, the more the number of the expanded feature maps, consequently, the RM network can extract more information from different angles, which improves the performance of the network. However, with the increase of rotation angle, interpolation error is introduced during expanding and realigning stages, and the feature extraction ability of CNN is fluctuant with the rotation interval θ down. In addition, The influence of the interpolation error will also be related to the size of the feature map where RM is located. The feature maps with small size are more easily influenced by the error than the big ones. This is why in Table 4, 45-degree intervals do not have a significant advantage over 90-degree. Considering a non-90-degree rotation interval increases the calculation complexity and causes interpolation error, while the classification improvement of a 90-degree is also significant and easy to be implemented, we chose 90-degree as the rotation interval in the later experiments.

Table 4: The classification results of different rotation intervals

Network	AP (%)	Ave Sen (%)	Ave Spec (%)
Baseline	56.20	70.86	96.93
90	64.07	75.32	97.17
60	64.40	74.06	96.83
45	65.66	73.33	96.92

4.5. Embedding an RM in Different CNNs

4.5.1. Embedding an RM in Different Stages of CNNs

RM is a general operation and can be easily added to different networks. Table 5 gives the classification results when embedding an strict RM-GAP structure in different CNNs, where i_j denotes combining an RM from the starting stage $i^{\prime}h$ to the last convolution structure $j^{\prime}h$ before GAP (ResNet34 contains 16 residual blocks, GoogleNet-Inception-V3 contains five types of Inception modules from A to E and EfficientNet-b0 contains 9 stages where stage 2 to 8 are MBConv modules). It can be seen that, after an RM is embedded, these networks obtained better performance than their baselines, which shows that our RM structure can indeed extract more effective features. Moreover, inserting RM from the middle of the network can obtain better results. This is because, different starting positions and different sizes of feature maps make the RM network get different levels of semantic information. In the shallow layers, the extracted features are relatively low-level, while in the deep layers, feature maps have small spatial size and the precise spatial information is lost. Relatively, the feature maps in middle layers of the network contain appropriate semantic information and their sizes are also moderate. Therefore, the middle layers of CNNs may be better positions to be combined with the RM.

4.5.2. Comparison Between Relaxed RM-GAP Structure and Strict RM-GAP Structure

Figure 2 (b) is a relaxed RM-GAP structure. Although the structure is not strictly rotation-invariant, it can still improve the anti-rotation ability of the network. In this part, we compare the effects of relaxed RM-GAP structure and strict RM-GAP structure by embedding RM operations into different CNNs, and select the best result of the two methods for comparison. The experimental results in Table 6 show that embedding the relaxed RM structure into the network also improves the feature extraction ability of the CNNs, but the improvement effect is not as good as the strict structure. Embedding relaxed RM-GAP structure, the features extracted by the network only have rotation equivariance, weak anti-rotation ability, and low robustness to rotation transformation.

4.6. Comparison with Other Rotation Invariance or Equivariance Methods

Taking the ResNet18 as baseline network, we compared our RM network with five classic rotation invariance or equivariance methods including rotation data augment (RA), TI-pooling [31], STN[39], ORN[36] and GCNN[35] methods in dermoscopy image classification task. For a fair comparison, we retrained these compared methods on ISIC 2019 dataset. RA and TI-pooling methods need to rotate the input image, while ORN and GCNN methods rotate the filters, and in this paper, all the rotation intervals of these methods were set to 90-degree. In addition, similar to our RM, STN, ORN, and GCNN models can also be easily inserted into different parts of the networks, so we selected the best classification results of different methods and compared them. Table 7 gives the classification results on the testing dataset. It can be seen that RA, TI-pooling, and STN can improve the performance of the network, while ORN and GCNN obtained lower metrics.

RA operation increases the sample diversity by rotating the training samples to improve the network generalization ability. TI-pooling used the parallel network architecture to learn the anti-rotation features, which shared almost the whole baseline network frame from the input layer to the full connection layer, so it cannot be flexibly inserted in different parts of the baseline network. STN, ORN, and GCNN can be inserted into each position of the network. STN is inserted into the network as a learning module, which can adaptively learn different spatial transformations among the data. But STN is not mainly designed for rotation transformation and there is no strict rotation invariance, so the improvement is limited. In addition, most metrics of ORN and GCNN are reduced, which may prove that the method of rotating convolution kernel introduces large interpolation error and reduces the feature extraction ability

Table 5: The classification results of embedding a strict RM-GAP structure in different CNNs.

Network	AP (%)	Ave Sen (%)	Ave Spec (%)
ResNet18			
Baseline	56.20	70.86	96.93
1_8	61.80	72.38	96.96
3_8	61.11	73.91	96.89
5_8	64.07	75.32	96.31
7_8	58.34	73.41	96.84
ResNet34			
Baseline	57.83	70.85	96.88
1_16	62.96	70.53	96.91
4_16	61.40	68.75	96.89
8_16	66.76	75.43	97.08
12_16	66.25	75.84	97.10
14_16	61.40	68.04	96.76
GoogleNet-Inception-V3			
Baseline	53.68	63.40	95.62
A.E	65.81	74.66	96.37
B.E	63.14	67.25	95.58
C.E	69.08	74.86	97.28
D.E	68.38	70.19	97.02
EfficientNet-b0			
Baseline	66.03	76.75	97.50
2_9	67.33	77.24	97.37
4_9	68.96	78.50	97.45
5_9	70.06	76.99	97.40
6_9	68.45	78.18	97.52
8_9	67.16	75.79	97.53

of the network for dermoscopy images. When they are inserted into a layer of the network, they may change the network structure, resulting in difficulty in using transfer learning for training. In terms of a single category, almost all evaluations of our method are better than other methods. Only the classification sensitivity of the VASC category is lower than that of baseline and STN, which is in the middle position, and this type of dermoscopy image only accounts for 1% of the total number.

Figure 5 shows the receiver operating characteristic (ROC) curve and the area under the curve (AUC) of the overall model and 8 types of skin disease classification results using different methods. It can be seen that each ROC curve of our method is closer to the upper left corner of the distance, and the classification performance is better. Relative to the five compared methods, the ROC curves under the RM method are more compact, which proves that RM can effectively improve the feature learning ability of the network. For the problem of the imbalanced dataset, the classification performance of a small number of categories can be improved. Relative to the five compared methods, RM network has achieved better performance on the classification task. The AP of our method exceeds the baseline network by 8.07% and is 6.15% higher than those of compared methods, while Ave Sen is 4.46% and 2.93%, respectively. At the same time, the Kappa consistency has also been greatly improved, close to a high degree (Kappa 0.74, close to 0.75). Therefore, with significant improvement, our method outperformed the compared methods.

Table 6: The classification results compared relaxed RM-GAP structure and strict RM-GAP structure in different CNNs.

Network	AP (%)	Ave Sen (%)	Ave Spec (%)
ResNet18			
Baseline	56.20	70.86	96.93
Relax	58.12	65.70	96.31
Strict	64.07	75.32	97.17
ResNet34			
Baseline	57.83	70.85	96.88
Relax	60.03	73.63	96.93
Strict	66.76	75.43	97.08
GoogleNet-Inception-V3			
Baseline	53.68	63.40	95.62
Relax	62.92	70.85	96.61
Strict	69.08	74.86	97.28
EfficientNet-b0			
Baseline	66.03	76.75	97.50
Relax	69.09	76.14	97.33
Strict	70.06	76.99	97.40

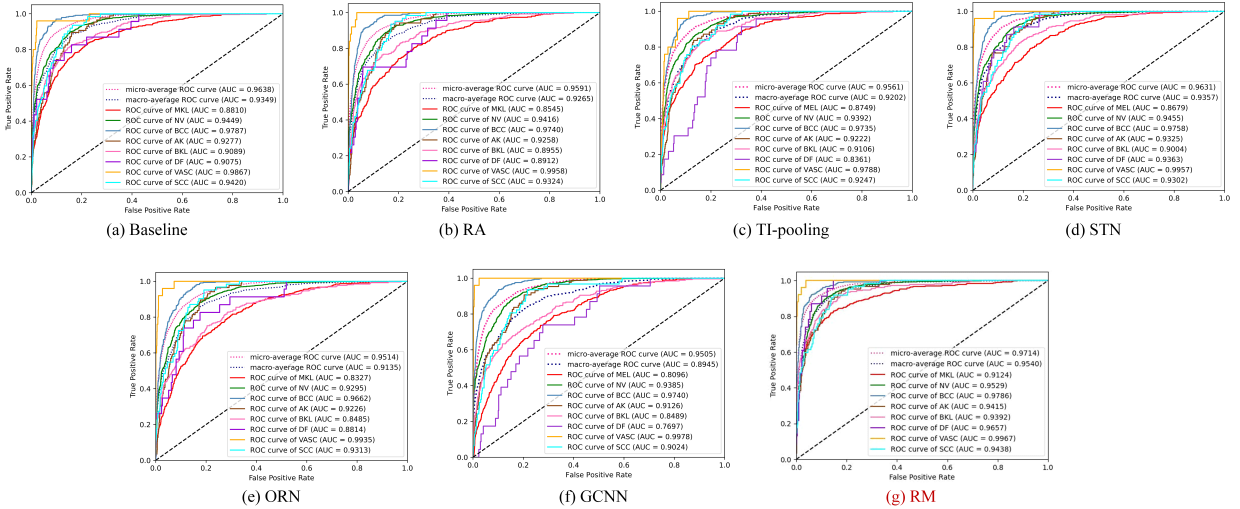


Figure 5: ROC curves of different anti-rotation methods: The figure shows the ROC curves and the AUC of the overall model and 8 types of skin disease classification results.

4.7. Comparison with Other Dermoscopy Image Classification Methods

From the above experiments, we have used the classic CNNs and compared it with the network after inserting RM. In this part of the experiments, we compare with some recent methods designed for skin lesion classification task. We chose the classification method based on the basic network, ARLNets[15] and RegNets[14; 27]. ARLNets is designed based on ResNets for dermoscopy classification. The residual attention module improves the network’s ability to represent skin lesions. Yao *et al.*[14] recently used the RegNets[27] to extract features for the first time in the dermoscopic image classification task, and achieved better performance than other classic CNNs, and designed a multi-weighted new loss (MWNL) method for imbalanced small dermoscopy datasets.

Table 7: The classification results of different rotation invariance or equivariance methods(%).

Disease category	Methods(%)						
	Baseline	RA	TI-pooling	STN	ORN	GCNN	RM
MEL							
Precision	71.02	61.95	63.05	67.04	59.51	63.94	72.57
Sensitivity	75.00	76.52	76.20	76.90	72.70	75.06	78.47
Specificity	93.76	92.47	92.25	93.02	91.52	92.40	94.13
NV							
Precision	93.71	96.11	94.17	94.72	95.10	94.48	93.55
Sensitivity	87.45	84.09	85.29	85.30	81.87	83.57	88.33
Specificity	92.96	93.44	93.23	93.82	93.91	93.39	92.88
BCC							
Precision	87.35	89.46	86.45	88.55	84.94	87.95	89.16
Sensitivity	77.96	75.94	73.97	77.37	72.12	72.28	78.10
Specificity	98.05	97.77	97.90	98.23	97.66	98.12	98.33
AK							
Precision	26.74	25.58	24.42	30.23	20.93	18.60	37.21
Sensitivity	53.49	52.38	55.26	57.78	51.43	59.26	56.14
Specificity	97.47	97.43	97.39	97.58	97.27	97.20	97.82
BKL							
Precision	67.18	59.92	64.12	59.92	52.29	58.40	70.99
Sensitivity	67.69	68.31	68.57	69.16	69.90	71.16	75.30
Specificity	96.21	95.80	95.88	95.44	94.64	95.29	96.67
DF							
Precision	13.04	26.09	26.09	13.04	8.70	8.70	30.43
Sensitivity	50.00	75.00	75.00	60.00	66.67	66.67	70.00
Specificity	99.21	99.21	99.33	99.21	99.17	99.17	99.36
VASC							
Precision	68.00	72.00	76.00	76.00	60.00	80.00	88.00
Sensitivity	94.44	85.00	86.36	95.00	88.24	90.91	91.67
Specificity	99.68	99.68	99.76	99.76	99.60	99.80	99.88
SCC							
Precision	22.58	29.03	30.65	25.81	20.97	14.52	32.26
Sensitivity	60.87	61.90	57.58	55.17	59.09	50.00	64.52
Specificity	98.08	98.05	98.28	98.16	98.05	97.89	98.32
Total							
AP	56.20	57.52	58.12	56.91	50.30	53.32	64.27
Ave Sen	70.86	72.39	72.28	72.08	69.53	71.11	75.32
Ave Spe	96.93	96.73	96.75	96.90	96.34	96.48	97.17
Kappa	71.36	69.85	69.16	70.28	64.15	65.06	74.20

To ensure the fairness of comparison, we retrain the networks of compared methods on ISIC2019 dataset. In

Table 8: The performance of other dermoscopy image classification methods.

Network	AP (%)	Ave Sen (%)	Ave Spec (%)	Kappa (%)
ARLNet18	59.33	72.58	96.92	70.89
ResNet18_RM	64.27	75.32	97.17	74.20
ARLNet34	60.21	74.94	96.75	70.16
ResNet34_RM	66.76	75.43	97.08	73.78
RegNetY800M	65.62	76.68	97.24	73.61
RegNetY800M_RM	70.08	77.99	97.44	76.21
RegNetY800M_MWNL	77.02	78.02	97.34	77.01
RegNetY800M_MWNL_RM	78.87	79.26	97.51	78.56

Table 9: The retrieval performance of RM networks in different CNNs.

Network	mAP@10(%)	mRR@10(%)
ResNet18	53.82	62.03
ResNet18_RM	64.38	67.25
ResNet34	61.57	68.92
ResNet34_RM	65.15	71.25
Inception-V3	59.67	66.70
Inception-V3_RM	67.34	74.11

addition, we use the same baseline for different methods and embed the RM structure into them. In the comparison of the first three groups in Table, we used the same hyperparameters and weighted cross-entropy loss as the above experiments. It can be seen that our method performs better. Then, in the last group, RegNetY800M_MWNL means using the MWNL loss function for training, and the training details are the same as that in [14]. It can be seen that applying our structure to this method can also obtain better classification results, and our module has great universality.

4.8. Using RM in Dermoscopy Image Retrieval Task

Dermoscopy image retrieval technology is an effective method to assist doctors in diagnosis. Doctors can get some reference information for diagnosis by retrieving similar dermoscopy images and their diagnosis reports in the database. In recent years, the highly robust dermoscopy image retrieval algorithm based on deep hashing using CNN is gradually replacing the traditional retrieval algorithm using manually designed features [16]. The proposed RM can also be applied to the retrieval task of dermoscopy images.

4.8.1. Verification of RM in Retrieval Task

This part of the experiment adopts the deep hashing method. Refer to [50] to insert a full connection layer before ResNet18, ResNet34, and GoogLeNet-Inception-V3 network classification layers as the hash code generation layer. The number of neurons in this layer is the number of bits of the hash code. We choose 16 bits as hash code bits and use cosine distance as similarity measure function. The RM embedding position is the same as the best performing network in Table 6. The performance of RM network on dermoscopy image retrieval task is verified on ISIC 2019 dataset. The training set is used to build the database, the images in the testing set are used as the query images. We also use weighted cross entropy loss during training. As can be seen from the Table 9, the network with the RM inserted can extract deep hash codes with rotation invariance and perform well on retrieval tasks.

4.8.2. Comparison with Other Retrieval Methods

We compared other retrieval methods for natural images and dermoscopy images, including natural image retrieval methods DCH [51], DPN[52] and CSQ [53], and dermoscopy image retrieval method CRI [16]. The methods

above all improve the loss function to make the intra-class distribution of the learned depth hash code more compact. Among them, CRI method also considers that the type of skin lesions does not change due to the imaging angle, and proposes an anti-rotation loss term based on the Cauchy distribution probability function. This method obtains certain rotation invariance by rotating the input image at equal intervals and learning the output differences of samples at different angles. In order to ensure the fairness of the experiment, we use ResNet18 as the baseline and the method of constructing a deep hashing network is the same as the previous experiment.

Table 10: The performance of other image retrieval methods.

Network	mAP@10(%)	mRR@10(%)
Baseline	53.82	62.03
DCH	55.10	63.62
DPN	55.30	65.14
CSQ	55.65	66.31
CRI	60.35	65.49
RM	64.38	67.25

Table 10 show the performance of our method and other retrieval methods. As can be seen, our method and CRI perform better than other comparison algorithms, indicating that the anti-rotation method can significantly improve the network’s ability to extract features from a large number of rotations in the dermoscopy dataset, and is more suitable for dermoscopy image retrieval task. Compared with the baseline, mAP@10 and mRR@10 of our method are improved by 10.56% and 5.22%, respectively; compared with the CRI method, which is also based on improving anti-rotation ability of networks, mAP@10 and mRR@10 by 4.03% and 1.76% respectively. It is proved that the features are rotation invariant after embedding RM operation, and the feature extraction ability of CNNs is greatly improved compared with the methods based on loss. Moreover, our method only used for partial convolution structure. Compared with the CRI method using the entire siamese network, the amount of computation is lower under the same rotation intervals.

5. Conclusion

CNNs have been widely used in the assisted diagnosis of dermoscopy images and achieved significant results. However, CNNs usually have weak anti-rotation abilities and there are a large number of skin lesion target rotations in the dermoscopy dataset. In this paper, a general anti-rotation model RM is proposed for dermoscopy images, which can be used in classification and retrieval tasks. Through theoretical derivation, the proposed RM can extract rotation-invariant features when being followed by a GAP operation. Our method is a general operation and can be flexibly embedded in any part of a standard CNN, which does not change the network structure or increase the parameters. Taking popular networks including ResNet18, ResNet34, GoogleNet-Inception-V3, and EfficientNet-b0 as baseline networks respectively, qualitative and quantitative experiments were carried out on ISIC 2019 dataset. Through experiments, the influence factors on the RM, such as the embedding position, the rotation interval, etc., were systematically discussed, which provides a reference to the readers for better using our RM. Compared with other classic rotation invariance or equivariance methods, our method can more effectively improve the performance and also outperforms the compared algorithms in the classification task and retrieval task.

In addition, we also tried to use RM in the skin lesion segmentation task. Because the segmentation network does not use GAP layer and rotation equivariance is more important than invariance in segmentation, only a relaxed RM structure can be used. The experimental results show that the improvement of the network is not obvious, so this task was not adopted. The potential of RM in the segmentation task needs to be further explored.

6. Acknowledgements

This work was supported by the National Natural Science Foundation of China (Nos. 61871011, 82173449, 62071011 and 61971443), the Beijing Municipal Natural Science Foundation (No. 4192032).

References

- [1] D. Yang, M. Chen, Y. Sun, Y. Jin, C. Lu, X. Pan, G. Quan, C. Wu, Microneedle-mediated transdermal drug delivery for treating diverse skin diseases, *Acta Biomaterialia* 121 (2021) 119–133.
- [2] R. L. Siegel, K. D. Miller, A. Jemal, *Cancer statistics, 2019, CA: a cancer journal for clinicians* 69 (1) (2019) 7–34.
- [3] M. Vestergaard, P. Macaskill, P. Holt, S. Menzies, Dermoscopy compared with naked eye examination for the diagnosis of primary melanoma: a meta-analysis of studies performed in a clinical setting, *British Journal of Dermatology* 159 (3) (2008) 669–676.
- [4] H. Kittler, H. Pehamberger, K. Wolff, M. Binder, Diagnostic accuracy of dermoscopy, *The lancet oncology* 3 (3) (2002) 159–165.
- [5] H. Zhou, F. Xie, Z. Jiang, J. Liu, S. Wang, C. Zhu, Multi-classification of skin diseases for dermoscopy images using deep learning, in: *2017 IEEE international conference on imaging systems and techniques (IST)*, IEEE, 2017, pp. 1–5.
- [6] B. Cassidy, C. Kendrick, A. Brodzicki, J. Jaworek-Korjakowska, M. H. Yap, Analysis of the isic image datasets: Usage, benchmarks and recommendations, *Medical image analysis* 75 (2022) 102305.
- [7] I. Maglogiannis, C. N. Doukas, Overview of advanced computer vision systems for skin lesions characterization, *IEEE transactions on information technology in biomedicine* 13 (5) (2009) 721–733.
- [8] P. Schmid-Saugeona, J. Guilloidb, J.-P. Thirana, Towards a computer-aided diagnosis system for pigmented skin lesions, *Computerized Medical Imaging and Graphics* 27 (1) (2003) 65–78.
- [9] N. K. Mishra, M. E. Celebi, An overview of melanoma detection in dermoscopy images using image processing and machine learning, *arXiv preprint arXiv:1601.07843* (2016).
- [10] F. Xie, H. Fan, Y. Li, Z. Jiang, R. Meng, A. Bovik, Melanoma classification on dermoscopy images using a neural network ensemble model, *IEEE transactions on medical imaging* 36 (3) (2016) 849–858.
- [11] Y. Xie, J. Zhang, Y. Xia, C. Shen, A mutual bootstrapping model for automated skin lesion segmentation and classification, *IEEE transactions on medical imaging* 39 (7) (2020) 2482–2493.
- [12] J. Kawahara, A. BenTaieb, G. Hamarneh, Deep features to classify skin lesions, in: *2016 IEEE 13th international symposium on biomedical imaging (ISBI)*, IEEE, 2016, pp. 1397–1400.
- [13] L. Yu, H. Chen, Q. Dou, J. Qin, P.-A. Heng, Automated melanoma recognition in dermoscopy images via very deep residual networks, *IEEE transactions on medical imaging* 36 (4) (2016) 994–1004.
- [14] P. Yao, S. Shen, M. Xu, P. Liu, F. Zhang, J. Xing, P. Shao, B. Kaffenberger, R. X. Xu, Single model deep learning on imbalanced small datasets for skin lesion classification, *IEEE Transactions on Medical Imaging* 41 (5) (2021) 1242–1254.
- [15] J. Zhang, Y. Xie, Y. Xia, C. Shen, Attention residual learning for skin lesion classification, *IEEE transactions on medical imaging* 38 (9) (2019) 2092–2103.
- [16] Y. Zhang, F. Xie, X. Song, Y. Zheng, J. Liu, J. Wang, Dermoscopic image retrieval based on rotation-invariance deep hashing, *Medical Image Analysis* (2021) 102301.
- [17] S. Allegretti, F. Bolelli, F. Pollastri, S. Longhitano, G. Pellacani, C. Grana, Supporting skin lesion diagnosis with content-based image retrieval, in: *2020 25th International Conference on Pattern Recognition (ICPR)*, IEEE, 2021, pp. 8053–8060.
- [18] L. Bi, J. Kim, E. Ahn, D. Feng, Automatic skin lesion analysis using large-scale dermoscopy images and deep residual networks, *arXiv preprint arXiv:1703.04197* (2017).
- [19] X. Zhang, L. Liu, Y. Xie, J. Chen, L. Wu, M. Pietikainen, Rotation invariant local binary convolution neural networks, in: *Proceedings of the IEEE International Conference on Computer Vision (ICCV) Workshops*, 2017.
- [20] P. Tschandl, C. Rosendahl, H. Kittler, The ham10000 dataset, a large collection of multi-source dermatoscopic images of common pigmented skin lesions, *Scientific data* 5 (1) (2018) 1–9.
- [21] N. C. Codella, D. Gutman, M. E. Celebi, B. Helba, M. A. Marchetti, S. W. Dusza, A. Kalloo, K. Liopyris, N. Mishra, H. Kittler, et al., Skin lesion analysis toward melanoma detection: A challenge at the 2017 international symposium on biomedical imaging (isbi), hosted by the international skin imaging collaboration (isic), in: *2018 IEEE 15th international symposium on biomedical imaging (ISBI 2018)*, IEEE, 2018, pp. 168–172.
- [22] M. Combalia, N. C. Codella, V. Rotemberg, B. Helba, V. Vilaplana, O. Reiter, C. Carrera, A. Barreiro, A. C. Halpern, S. Puig, et al., Bcn20000: Dermoscopic lesions in the wild, *arXiv preprint arXiv:1908.02288* (2019).
- [23] A. Krizhevsky, I. Sutskever, G. E. Hinton, Imagenet classification with deep convolutional neural networks, *Advances in neural information processing systems* 25 (2012) 1097–1105.
- [24] K. He, X. Zhang, S. Ren, J. Sun, Deep residual learning for image recognition, in: *Proceedings of the IEEE conference on computer vision and pattern recognition*, 2016, pp. 770–778.
- [25] J. Hu, L. Shen, G. Sun, Squeeze-and-excitation networks, in: *Proceedings of the IEEE conference on computer vision and pattern recognition*, 2018, pp. 7132–7141.
- [26] M. Tan, Q. Le, Efficientnet: Rethinking model scaling for convolutional neural networks, in: *International Conference on Machine Learning*, PMLR, 2019, pp. 6105–6114.
- [27] I. Radosavovic, R. P. Kosaraju, R. Girshick, K. He, P. Dollár, Designing network design spaces, in: *Proceedings of the IEEE/CVF Conference on Computer Vision and Pattern Recognition*, 2020, pp. 10428–10436.
- [28] K. Sohn, H. Lee, Learning invariant representations with local transformations, *arXiv preprint arXiv:1206.6418* (2012).
- [29] A. Kanazawa, A. Sharma, D. Jacobs, Locally scale-invariant convolutional neural networks, *arXiv preprint arXiv:1412.5104* (2014).
- [30] D. A. Van Dyk, X.-L. Meng, The art of data augmentation, *Journal of Computational and Graphical Statistics* 10 (1) (2001) 1–50.
- [31] D. Laptev, N. Savinov, J. M. Buhmann, M. Pollefeys, Ti-pooling: transformation-invariant pooling for feature learning in convolutional neural networks, in: *Proceedings of the IEEE conference on computer vision and pattern recognition*, 2016, pp. 289–297.
- [32] J. Kim, W. Jung, H. Kim, J. Lee, Cycnn: A rotation invariant cnn using polar mapping and cylindrical convolution layers, *arXiv preprint arXiv:2007.10588* (2020).
- [33] M. Weiler, F. A. Hamprecht, M. Storath, Learning steerable filters for rotation equivariant cnns, in: *Proceedings of the IEEE Conference on Computer Vision and Pattern Recognition*, 2018, pp. 849–858.

- [34] D. Marcos, M. Volpi, D. Tuia, Learning rotation invariant convolutional filters for texture classification, in: 2016 23rd International Conference on Pattern Recognition (ICPR), IEEE, 2016, pp. 2012–2017.
- [35] T. Cohen, M. Welling, Group equivariant convolutional networks, in: International conference on machine learning, PMLR, 2016, pp. 2990–2999.
- [36] Y. Zhou, Q. Ye, Q. Qiu, J. Jiao, Oriented response networks, in: Proceedings of the IEEE Conference on Computer Vision and Pattern Recognition, 2017, pp. 519–528.
- [37] X. Cheng, Q. Qiu, R. Calderbank, G. Sapiro, Rotdcf: Decomposition of convolutional filters for rotation-equivariant deep networks, arXiv preprint arXiv:1805.06846 (2018).
- [38] M. Zareapoor, J. Chanussot, H. Zhou, J. Yang, et al., Rotation equivariant feature image pyramid network for object detection in optical remote sensing imagery (2021).
- [39] M. Jaderberg, K. Simonyan, A. Zisserman, et al., Spatial transformer networks, Advances in neural information processing systems 28 (2015) 2017–2025.
- [40] J. Dai, H. Qi, Y. Xiong, Y. Li, G. Zhang, H. Hu, Y. Wei, Deformable convolutional networks, in: Proceedings of the IEEE international conference on computer vision, 2017, pp. 764–773.
- [41] K. Qi, C. Yang, C. Hu, Y. Shen, S. Shen, H. Wu, Rotation invariance regularization for remote sensing image scene classification with convolutional neural networks, Remote Sensing 13 (4) (2021) 569.
- [42] J. Xu, X. Tang, Y. Zhu, J. Sun, S. Pu, Sgmnet: Learning rotation-invariant point cloud representations via sorted gram matrix, in: Proceedings of the IEEE/CVF International Conference on Computer Vision, 2021, pp. 10468–10477.
- [43] L. Zhou, H. Zhao, J. Leng, Mtcnet: Multi-task collaboration network for rotation-invariance face detection, Pattern Recognition 124 (2022) 108425.
- [44] C. Li, W. Wei, J. Li, J. Yao, X. Zeng, Z. Lv, 3dmol-net: learn 3d molecular representation using adaptive graph convolutional network based on rotation invariance, IEEE Journal of Biomedical and Health Informatics (2021).
- [45] X. Li, L. Yu, C.-W. Fu, P.-A. Heng, Deeply supervised rotation equivariant network for lesion segmentation in dermoscopy images, in: OR 2.0 Context-Aware Operating Theaters, Computer Assisted Robotic Endoscopy, Clinical Image-Based Procedures, and Skin Image Analysis, Springer, 2018, pp. 235–243.
- [46] C. Szegedy, V. Vanhoucke, S. Ioffe, J. Shlens, Z. Wojna, Rethinking the inception architecture for computer vision, in: Proceedings of the IEEE conference on computer vision and pattern recognition, 2016, pp. 2818–2826.
- [47] K. Lenc, A. Vedaldi, Understanding image representations by measuring their equivariance and equivalence, in: Proceedings of the IEEE conference on computer vision and pattern recognition, 2015, pp. 991–999.
- [48] R. J. Hunt, Percent agreement, pearson’s correlation, and kappa as measures of inter-examiner reliability, Journal of Dental Research 65 (2) (1986) 128–130.
- [49] L. Van der Maaten, G. Hinton, Visualizing data using t-sne., Journal of machine learning research 9 (11) (2008).
- [50] K. Lin, H.-F. Yang, J.-H. Hsiao, C.-S. Chen, Deep learning of binary hash codes for fast image retrieval, in: Proceedings of the IEEE conference on computer vision and pattern recognition workshops, 2015, pp. 27–35.
- [51] Y. Cao, M. Long, B. Liu, J. Wang, Deep cauchy hashing for hamming space retrieval, in: Proceedings of the IEEE Conference on Computer Vision and Pattern Recognition (CVPR), 2018.
- [52] L. Fan, K. Ng, C. Ju, T. Zhang, C. S. Chan, Deep polarized network for supervised learning of accurate binary hashing codes., in: IJCAI, 2020, pp. 825–831.
- [53] L. Yuan, T. Wang, X. Zhang, F. E. Tay, Z. Jie, W. Liu, J. Feng, Central similarity quantization for efficient image and video retrieval, in: Proceedings of the IEEE/CVF Conference on Computer Vision and Pattern Recognition, 2020, pp. 3083–3092.